Journal of Applied Fluid Mechanics, Vol. 16, No. 8, pp. 1654-1665, 2023.
Available online at www.jafmonline.net, ISSN 1735-3572, EISSN 1735-3645.
https://doi.org/10.47176/jafm.16.08.1661

Velocity Slip in a Deep-sea Slurry Pump and Its Effect on Particle Transportation

Y. Lv[1], X. Su[1,2,†], H. Yang[1], J. Zhang[1], R. Wang[1], and Z. Zhu[1]

[1] *Zhejiang Sci-Tech University, Hangzhou 310000, China*
[2] *Changsha Research Institute of Mining and Metallurgy, Co. Ltd., Changsha 410000, China*

†*Corresponding Author Email: suxianghui@sina.com*

ABSTRACT

The slurry pump, which forms the core equipment of the deep-sea mining (DSM) system, provides lifting power for the ore from the seabed to the sea level, which is crucial for the safety of coarse ore particle transportation. Velocity slip plays a significant role in revealing the migration of the pump particles. Therefore, this study analyzes the velocity slip in a slurry pump using the computational fluid dynamics–discrete element method (CFD-DEM) for the first time. The relationship between the pump head and velocity slip was proposed and verified in this study based on the velocity triangle and Euler equation of the solid-liquid two-phase flow in the impeller. The effects of different particle sizes on the velocity slip are compared in detail. According to the computational results, the head depends on the larger velocity slip of the impeller outlet and lower velocity slip at the inlet. The peak value of the velocity slip was significantly reduced, and the peak position of the velocity slip and zero-point position moved backward for particle sizes ranging between 5-15 mm. This study provides a reference for the problems of particle migration and velocity slip in slurry pumps.

Article History

Received November 19, 2022
Revised March 19, 2023
Accepted March 31, 2023
Available online May 31, 2023

Keywords:

Deep-sea mining
Slurry transport pump
CFD-DEM coupling
Solid-liquid two-phase flow
Velocity slip

1. INTRODUCTION

Slurry pumps used in deep-sea mining are vital equipment for transporting coarse particles and have a profound impact on the security of the lifting system and the economy, including hydraulic characteristics and geometric and running parameters. Among these parameters, the velocity slip is a crucial factor in the multiphase mechanism.

In recent years, scholars have studied the effects of various factors on particle velocity slip. Sun and Liu (2022) studied the velocity slip of large particles in vertical pipes and observed through experiments that the velocity slip increased and then decreased with the fluid flow rate and decreased with the particle volume concentration and fluid density. Li et al. (2016) used the PIV technique to derive that the velocity slip increased with the particle diameter and decreased with the particle volume concentration. Chen et al. (2021) concluded that the velocity slip increased with the flow velocity in a centrifugal pump at the same rotational speed and increased with rotational speed at different rotational speeds. Ning et al. (2022) showed that the velocity slip of particles increased first and remained in the elbow, and the velocity slip amplitude decreased with the curvature radius of the elbow.

Other studies have highlighted the effect of velocity slip on the pump, and the velocity slip coefficient is a critical factor affecting the predicted pump efficiency (Pei et al., 2021). Peng et al. (2021b) found that the viscosity of a solid-liquid two-phase flow increased, but the head and efficiency decreased with increasing numbers of particles. Peng et al. (2021a) studied the wear of the impeller and concluded that the velocity slip of the particles near the vane outlet gradually increased with concentration, affecting the wear position in the impeller.

Numerous researchers have extensively analyzed solid-liquid two-phase flow and particle movement. Tang and Kim (2020) reported that the smaller particles in a single-channel pump had a broader speed range and limiting velocity, while larger particles were characterized by greater contact force. Dong et al. (2017) argued that the crystal particles in the pump were evenly distributed at the inlet. The particles entered the impeller, and it was observed that the density was low on the suction side of the blade and high on the pressure side. Li et al. (2019) argued that increasing the impeller speed improved the

Nomenclature

C_D	particle resistance coefficient	u_s	particle velocity
C_m	the mass concentration of the solid	v_{u2s}	axial velocity component of the solid phase at the impeller outlet
d	particle size	v_{u2f}	axial velocity component of the liquid phase at the impeller outlet
F_D	resistance of particles	ρ	density
H	head of the pump	Δu	velocity slip
Q_d	flow rate of the pump	CFD	computational fluid dynamics
n	Rotating speed of the pump	DEM	discrete element method
u_f	fluid velocity	DSM	deep-sea mining

passing rate of the particles and reduced the extension of collision between particles. Liu et al. (2019a) found that the pump functioned more stably and that the efficiency and head were more reasonable by using CFX numerical simulations at a particle concentration of 10%. Hong et al. (2016) concluded that particles would minimize wear on blades if the profile of the blades was near the traces of particle movement. Liu et al. (2019b) found that increasing the pump flow rate improved the fluidity of particles and reduced the wear on the pump. Wen et al. (2019) considered the effects of various particle sizes on two-phase flow and revealed that a particle size of 10 mm had better adaptability to particle motion.

Previous studies on particle velocity slip and solid-liquid two-phase flow provide a good reference for this study. However, there is a lack of intuitive and data-based analyses of the velocity slip in slurry pumps in existing literature. This study monitored and extracted the two-phase flow velocity of the impeller and guide vane in a slurry pump at 5 mm intervals and compared the differences in velocity slip under three particle sizes of 5, 10, and 15 mm using numerical values. Therefore, this study discusses the influence of internal particle migration, velocity slip, and particle size on a typical slurry pump.

2. FORCES ON PARTICLES AND THE VELOCITY SLIP IN THE PUMP PERFORMANCE

The force acting on a particle is critical for altering its movement, and is also a factor that directly influences the value of velocity slip. The force on solid particles varies in different parts of the pump flow channel, resulting in different velocity slip values. In the impeller's solid-liquid two-phase velocity field, the fluid's equation of motion is given by (Wei 1997):

$$\rho_f \frac{du_f}{dt} = -\rho_f g_n Z + \rho_f \omega^2 r - 2\rho_f \omega u_f - \nabla \mathrm{P} + \mu \Delta W_f - \frac{F_D}{1 - C_v} \tag{1}$$

The motion equation of the solid phase is:

$$\rho \frac{du_s}{dt} + C\rho_f \frac{d\Delta u}{dt} = \rho g_n Z + \rho \omega^2 r + \frac{u_s}{R} - 2\rho \omega u_s - \nabla \mathrm{P} + \frac{F_D}{1 - C_v} \tag{2}$$

According to Eq. (2), the particle movement in the impeller is related to the velocity slip. A larger velocity slip gradient corresponds to smaller particle acceleration when other forces remain the same.

In the guide vane, the main forces on the particles are gravity, drag force, and Basset force. The particle momentum is given in by Eq. (3), and the magnitude of the velocity slip at different positions primarily affects particle motion. The acceleration of the particles also increases when the velocity slip is larger.

$$m_p \frac{du_s}{dt} = m_p g + 3\pi \mu d \Delta u + \frac{3}{2} d^2 \rho_f \sqrt{\pi \nu} \int_{t_0}^{t} \frac{d\Delta u}{d\tau} \cdot \frac{1}{\sqrt{t - \tau}} \cdot d\tau \tag{3}$$

where d and ρ are the particle size and density, respectively; u_f, u_s are the fluid velocity and particle velocity, respectively; Δu is the velocity slip ($\Delta u = u_f - u_s$); F_D is the resistance of particles ($F_{\mathrm{D}} = \frac{\pi d^2}{8} C_D \rho_f \Delta u^2$); and C_D is the particle resistance coefficient.

According to the theory of impeller design, we draw the velocity triangle of the solid-liquid phases at the impeller (as shown in Fig. 1). Further, the theoretical pump head formula, Eq. (4) can be obtained using Euler's equation, which is then transformed to Eq. (5). This shows that the size of the pump head is related to the velocity slips of the impeller inlet and outlet, and the mass concentration of the solid. A larger velocity slip at the impeller outlet is associated with a smaller inlet velocity slip and higher head.

$$H_{Tm} = \frac{\omega}{g}\left[(1 - C_m)\left(v_{u2f} R_2 - v_{u1f} R_1\right) + C_m (v_{u2s} R_2 - v_{u1s} R_1)\right] \tag{4}$$

Transforming the above theoretical head H_{Tm} equation, we obtain:

$$H_{Tm} = \frac{\omega}{g}\left[\left(v_{u2f} R_2 - v_{u1f} R_1\right) + C_m R_2 \Delta u_2 - C_m R_1 \Delta u_1\right] \tag{5}$$

where v_{u2s} and v_{u2f} are the axial velocity components of the solid and liquid phases, respectively, at the impeller outlet, and C_m is the mass concentration of the solid.

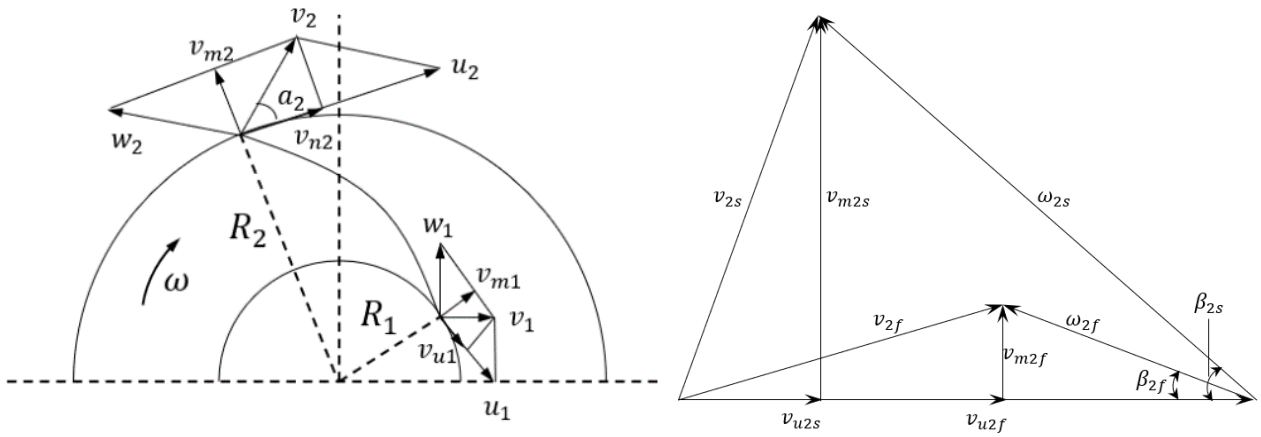

(a) (b)

Fig. 1 (a) Velocity triangle of the inlet and outlet of the impeller (b)Velocity triangle of solid-liquid two-phase flow in the impeller.

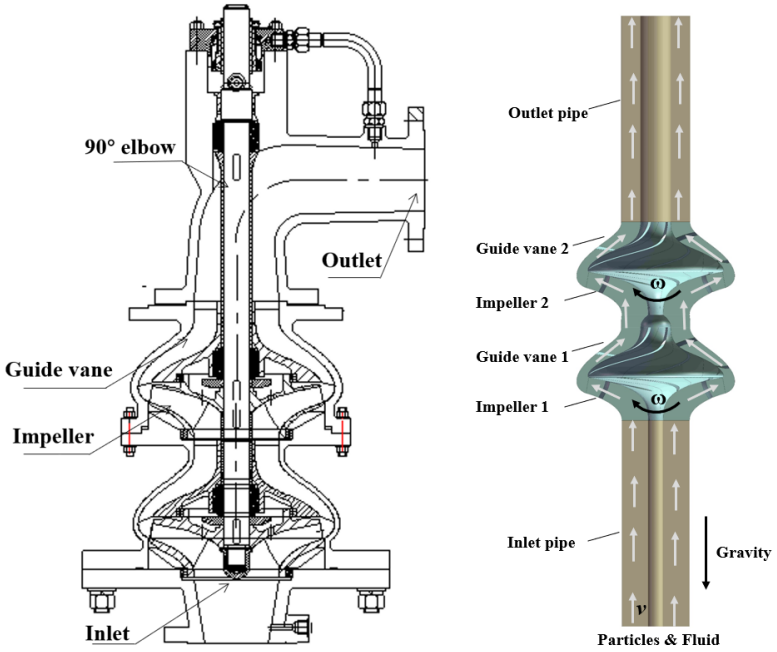

(a) Hydraulic model (b) 3D model

Fig. 2 Schematic of the slurry pump.

Table 1 Parameters of the slurry pump

Geometric parameters	Impeller	Guide vane	Working parameters	Value
Inlet diameter	135 mm	276 mm	Flow rate (Q_d)	120 m^3/h
Outer diameter	272 mm	38.5 mm	Head (H)	40 m
Number of blades	4	5	Rotating speed (n)	1450 rpm
Wrap angle	111°–115°	118°	Specific speed (n_s)	104

3. GEOMETRIC PARAMETERS AND NUMERICAL SETUP

3.1 Parameters of Slurry Transport pumps

This study focused on analyzing a slurry transport pump, which consisted of an inlet pipe, a first-stage pump, a second-stage pump (each stage pump comprising an impeller and a guide vane), and an outlet pipe. The hydraulic model of the slurry pump was presented in Fig. 2(a), and its geometric parameters were defined in Table 1. The solid-liquid two-phase flow's primary trajectory in the slurry pump was indicated by the gray arrow in Fig. 2(b). The working parameters of the primary and

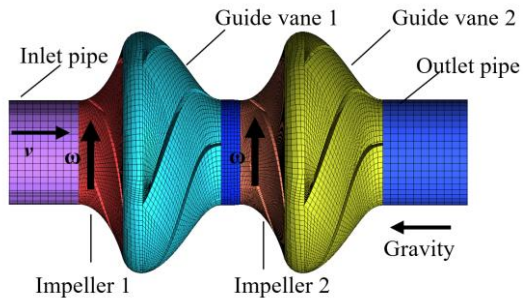

Fig. 3 Grid of the transport pump.

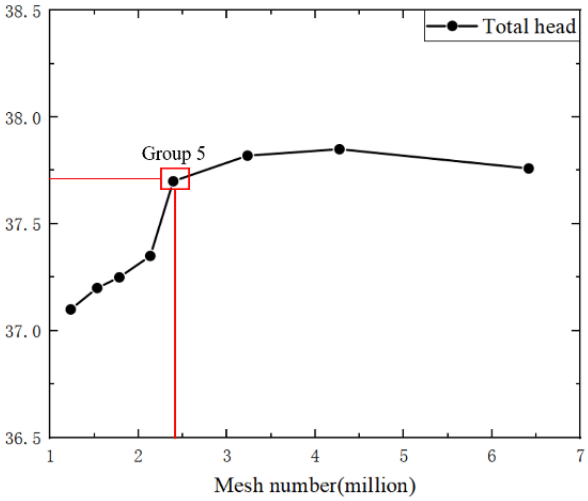

Fig. 4 Grid independence monitoring.

secondary rotating speeds and flow rates were provided in Table 1.

3.2 Mesh and Mesh Independence

The study employed the ICEM software to create structured grids for the computational domain, as depicted in Fig. 3. The orthogonality quality of the computational domain was ensured to be greater than 0.39. Eight sets of grids, ranging from 1.1 to 6.47 million, were established in this research. The relationship between the grid and head was calculated under the working flow rate of 120 m^3/h, as illustrated in Fig. 4. The grid independence analysis demonstrated that the total head of the pump did not increase significantly with the increase in the grid number when the grid number reached 2.39 million. Therefore, Group 5's grid size was considered appropriate for this study.

3.3 Numerical Setup

The CFD-DEM coupling method was used to simulate the two-phase solid–liquid flow. The water simulation was based on the computational fluid dynamics (CFD) method and was calculated using Fluent 2018. The transient realizable k-ε model was used for analyzing turbulence model, and the wall boundary condition was set to a non-slip wall with standard wall function. The inlet boundary condition used the velocity-inlet, while the outlet boundary was set as the outflow. The Navier-Stokes

Table 2 Interaction parameters

Interaction	Material recovery coefficient	Coefficient of static friction	Rolling friction coefficient
Particle-particle	0.44	0.27	0.01
Particles-pump	0.5	0.15	0.01

Table 3 Physical parameters

Objects	Density (kg/m^3)	Poisson's ratio	Shear modulus (MPa)
Particle	2000	0.4	21.3
Pump	7800	0.3	70

equation was solved using the SIMPLEC format. The time step was set to 3.432e-4 s, which corresponds to the time it takes for the impeller to rotate one degree. The gravitational acceleration was set to 9.81 m/s2 in the negative Z direction.

The simulation of the particles was based on the discrete element method (DEM) method and was calculated using EDEM. For the particle simulation, the Hertz-Mindlin model was used to calculate the contact force, and the interaction parameters in the contact model were shown in Table 2. The material properties of the pump and particles were set to aluminum alloy and artificial nodule, respectively, as shown in Table 3. Particle sizes were set to 5 mm, 10 mm, and 15 mm. To ensure accurate particle calculation, a shorter time step (20-30% of Rayleigh time step) was used within the fluid time step, which was set to 3.432e-5 s (21% of Rayleigh time step).

4. RESULTS AND DISCUSSION

This study analyzed the velocity slip relationship between the particles (three particle sizes of 5, 10, and 15 mm) and fluid in the slurry pump by monitoring the velocity information of the particles and the fluid every 5 mm in the axial direction of the slurry pump.

4.1 Experimental Verification and Performance Characteristics

The accuracy of the slurry pump calculation was verified by fitting the experimental results of Su et al. (2020). Figure 5 shows the observed and calculated performance curves of the slurry pump under different working conditions. The behavior of the pump, where the pump head decreases and efficiency improves as the flow rate increases gradually, was found to be consistent between the experimental results and numerical calculations. The slight numerical differences at the actual working point of 120 m^3/h as follows: in the mud condition, the head and efficiency differences are 0.49 m and 2.03%, respectively; in the water condition, the head and efficiency difference are 1.66 m and 2.46%, respectively. Overall, the correct numerical simulation

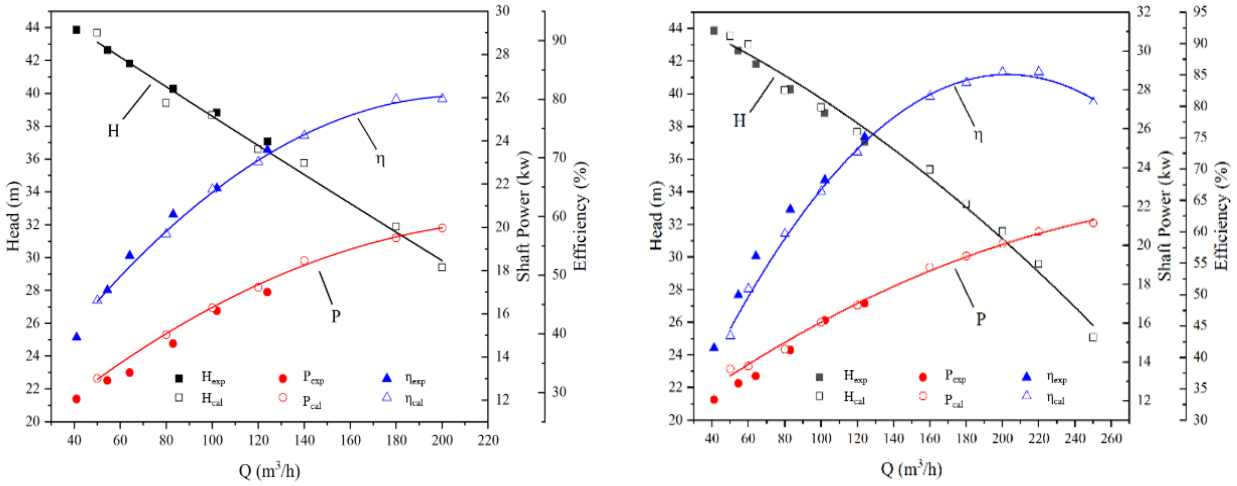

(a) Slurry condition (b) Water conditions

Fig. 5 Performance curve of slurry pump (Su et al., 2020).

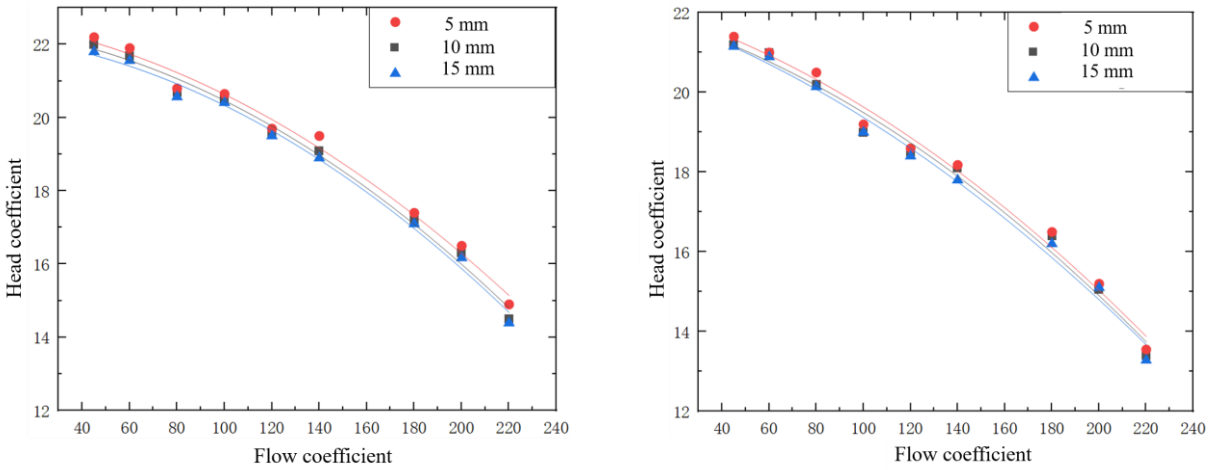

(a)First stage. (b)Second stage

Fig. 6 Performance curve of the pump under different particle sizes.

method was used in the study, indicating the accuracy of the slurry pump calculation.

In Section 2, the relationship between the pump head and solid-liquid velocity slip is obtained. Therefore, in this section this paper further calculates the external characteristic curves of the first-stage and second-stage pump under different particle sizes (as shown in Fig. 6). The head decreases with increasing particle size.

4.2 Flow Field and Particles Distribution in the Slurry Pump

This section discusses the velocity distributions of particles and fluid in a slurry transport pump. Figure 7 illustrates the spatial and velocity distributions of particles in the pump. At the entrance of the pump, agglomeration of particles occurs due to the low particles' velocity. As the particles enter the impeller, they are propelled by the impeller's rotation, and their velocity gradually increases until it reaches its maximum before leaving the impeller rapidly. However, as the particles reach the guide vane, they collide with the wall, and their speed decreases gradually. The particles then enter the second-stage impeller in an agglomerated form and at a higher velocity. The particle distributions in the first and second stages are quite similar.

The flow field distribution is closely related to the migration of the particles. Figure 8 illustrates the flow direction, which changes from the vertical direction of the input pipe to the radial motion of the impeller. As the fluid enters the primary impeller, the flow velocity increases from an average of 3 m/s to approximately 12 m/s, and then decreases gradually along the guide vane. At the inlet of the second-stage impeller, a vortex is formed due to the accelerated fluid, which causes the fluid to be squeezed.

To further investigate the flow velocity distribution in the pump and the trend of the flow lines (as shown in Fig. 9), it can be observed that the fluid experiences centrifugal force in the impeller and mainly clings to the vane near the suction surface. This leads to a lower velocity of the vane pressure surface and creates a vortex in the low-speed region. A similar phenomenon can also be observed in the guide vane. Consequently, the particles are affected by this and tend to move along the suction side of the guide vane blade.

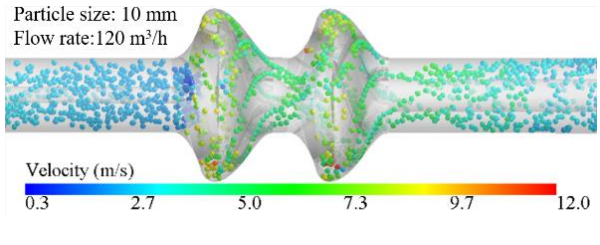

(a) Particle velocity distribution in the pump

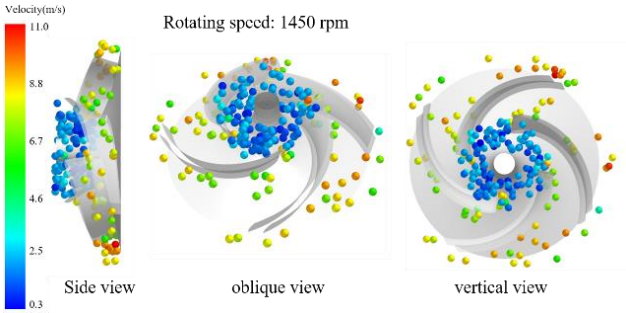

(b) Particle velocity distribution inside the impeller

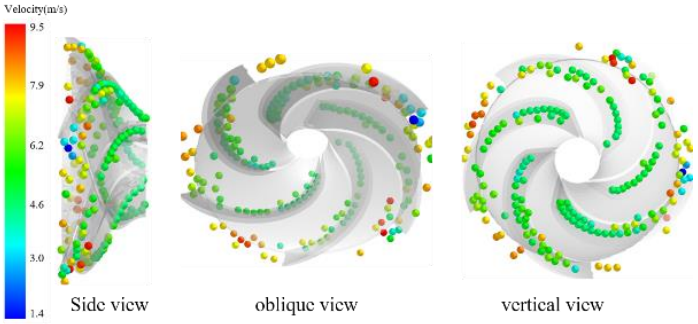

(c) Particle velocity distribution in the guide vane

Fig. 7 Particle velocity distribution in the slurry pump.

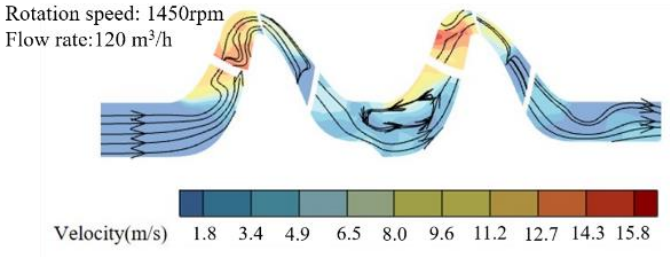

Fig. 8 Slurry pump shaft surface flow velocity distribution.

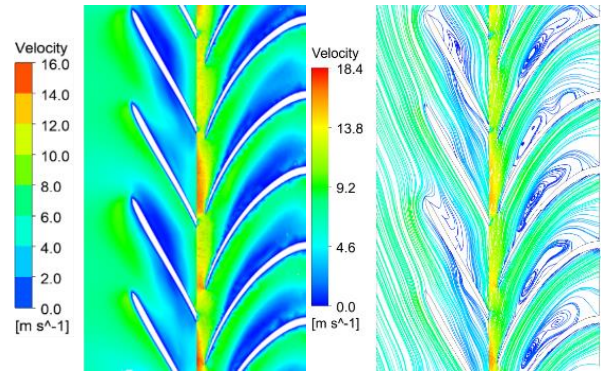

(a) First stage

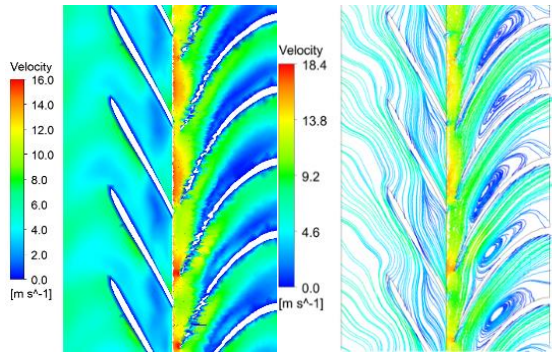

(b) Second stage

Fig. 9 Fluid relative velocity, flow line expansion diagram.

4.3 Comparison of Velocity Slip with Different Particle Sizes

Therefore, to further investigate the velocity relationship of the two-phase flow, Fig. 10 and 11 quantitatively monitor the two-phase flow velocity in the pump. In the first 10 mm along the axis, the speed of the particle is low and a large number of collision states (impeller inlet position) occur. The two-phase flow velocity difference is 0.47 m/s. Then, with the acceleration of the impeller rotation, the average velocity

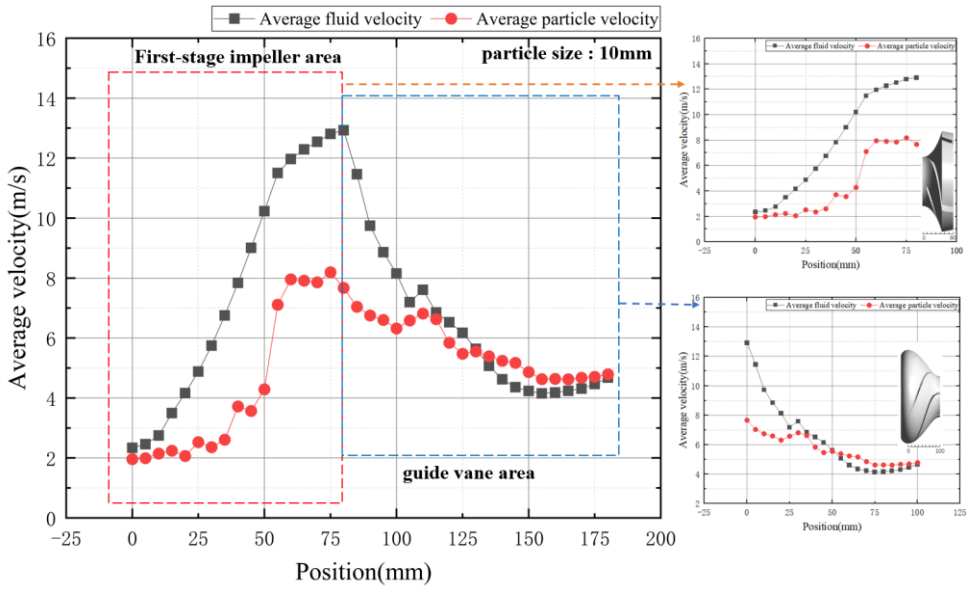

(a) Average fluid velocity and particle velocity in the first stage

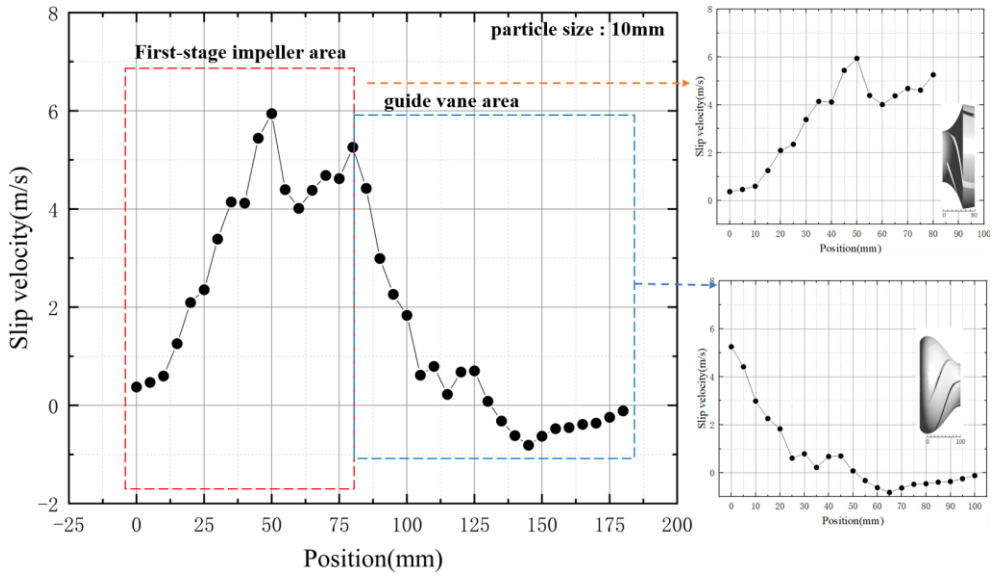

(b) Velocity slip in first stage

Fig. 10 Average particle-fluid velocity and velocity slip in the first stage.

of the particles and average fluid velocity display the same acceleration trend. From 10 mm to 55 mm, the two speeds increase linearly by approximately 0.2 times, while the velocity slip changes linearly by 0.13 times.

However, as the impeller flow channel diffusion increases, the velocity growth gradient decreases, the variation in the particle velocity tends to be flat, and the velocity slip oscillates in the interval of 4-6 m/s. When the two-phase flow enters the guide vane, the velocity of the flow field in the 80-130 mm interval decreases from 12.96 m/s to 5.5 m/s, and the velocity slip reduces from 5.26 m/s to 0.08 m/s. As the two-phase flow approaches the exit of the first-stage pump, the velocity of the particles is affected by deceleration much less than that of the fluid and exceeds the fluid velocity by an average of 0.44 m/s. From the above analysis, it can be concluded that, although the velocity trends of the two-phase flow in the pump are similar, the degree of increase or decrease differs significantly.

The velocity trends of the two-phase flow are similar during the first and second stages of the pump. However, the average particle velocity of 5.31 m/s and flow velocity of 6.26 m/s enters the impeller at a higher velocity than that of the first stage. As shown in Fig. 11, at the first 10 mm (impeller inlet position), the average velocity slip is 0.94 m/s which is double the inlet of the first stage. From 10 to 55 mm, the average particle velocity is less affected by the impeller. It has reached higher values maintained at around 5.3 m/s, so this results in a smooth increase in velocity slip.

As the impeller channel diffusion degree increased, the fluid velocity growth gradient decreased, the particle

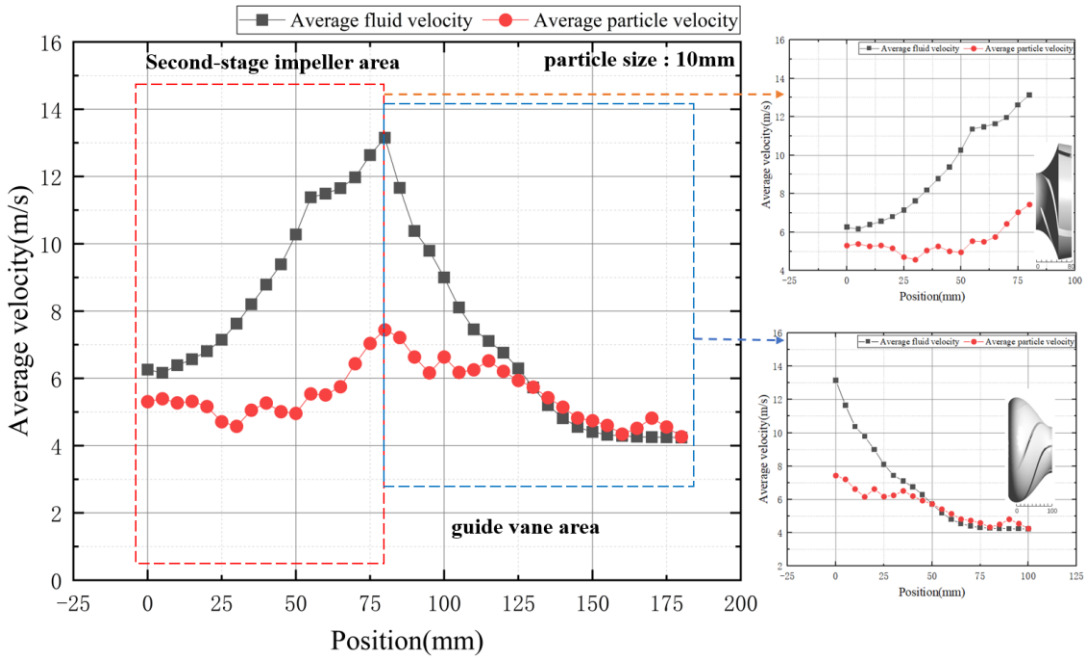

(a) Average fluid velocity and particle velocity in the second stage

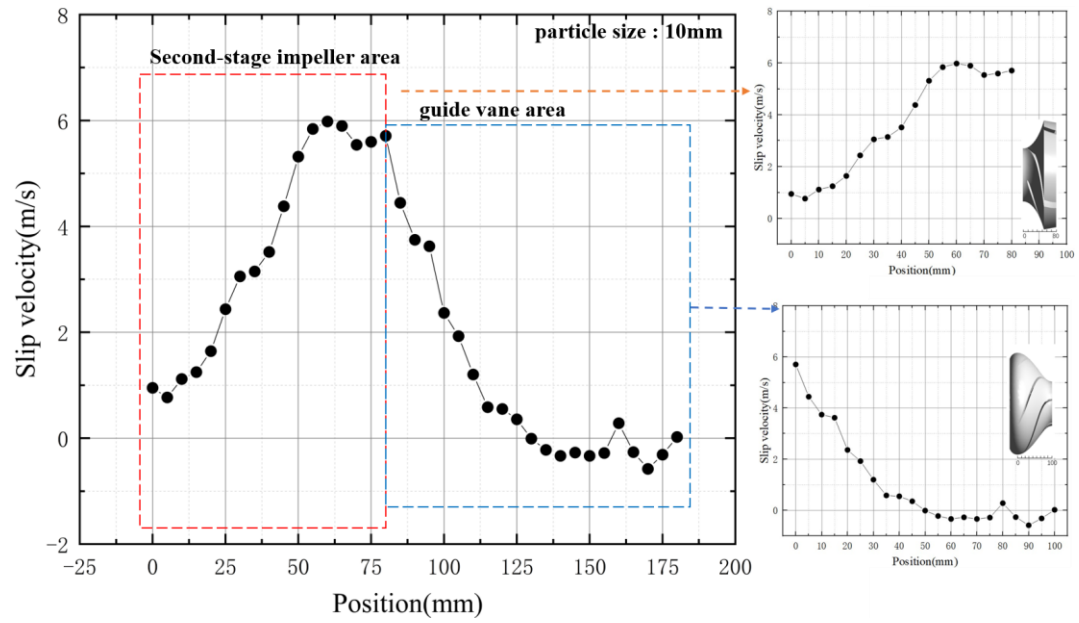

(b) Velocity slip in second stage.

Fig. 11 Average particle-fluid velocity and velocity slip in the second stage.

velocity reached a maximum value of 7.4 m/s, which was similar to that of the first stage, and the velocity slip between the two changed smoothly. When the two-phase flow entered the guide vane, the performance was similar to that of the first stage, and the velocity difference was approximately zero at the pump outlet.

To further study the velocity slip of particles in the pump, this paper analyzes the performance of particles with sizes of 5 mm and 15 mm. The effects of the three particle sizes on the velocity slip are compared.

When the particle size is reduced from 10 mm to 5 mm, the fluid velocity in Fig. 12(a) is compared with that in Fig. 10(a). The effect on the overall average fluid velocity is minimal, and the maximum fluid velocity at the impeller outlet has a difference of only 0.1 m/s compared to that of the 10 mm particles. In contrast, the difference in the velocity slip between the two-phase flows because of the influence of particle size on the movement of the particles is significant.

Figure 12(a) shows that the speed trajectory of the 5 mm particles in the impeller is smooth and close to the fluid velocity curve. The maximum velocity of 9.86 m/s is 28.3% higher than that of the 10 mm particles and the velocity of the particles at the exit of the guide vane is 5.59 m/s, which is 47.9% higher than that of the 10 mm particles. The effect of impeller channel diffusion on the

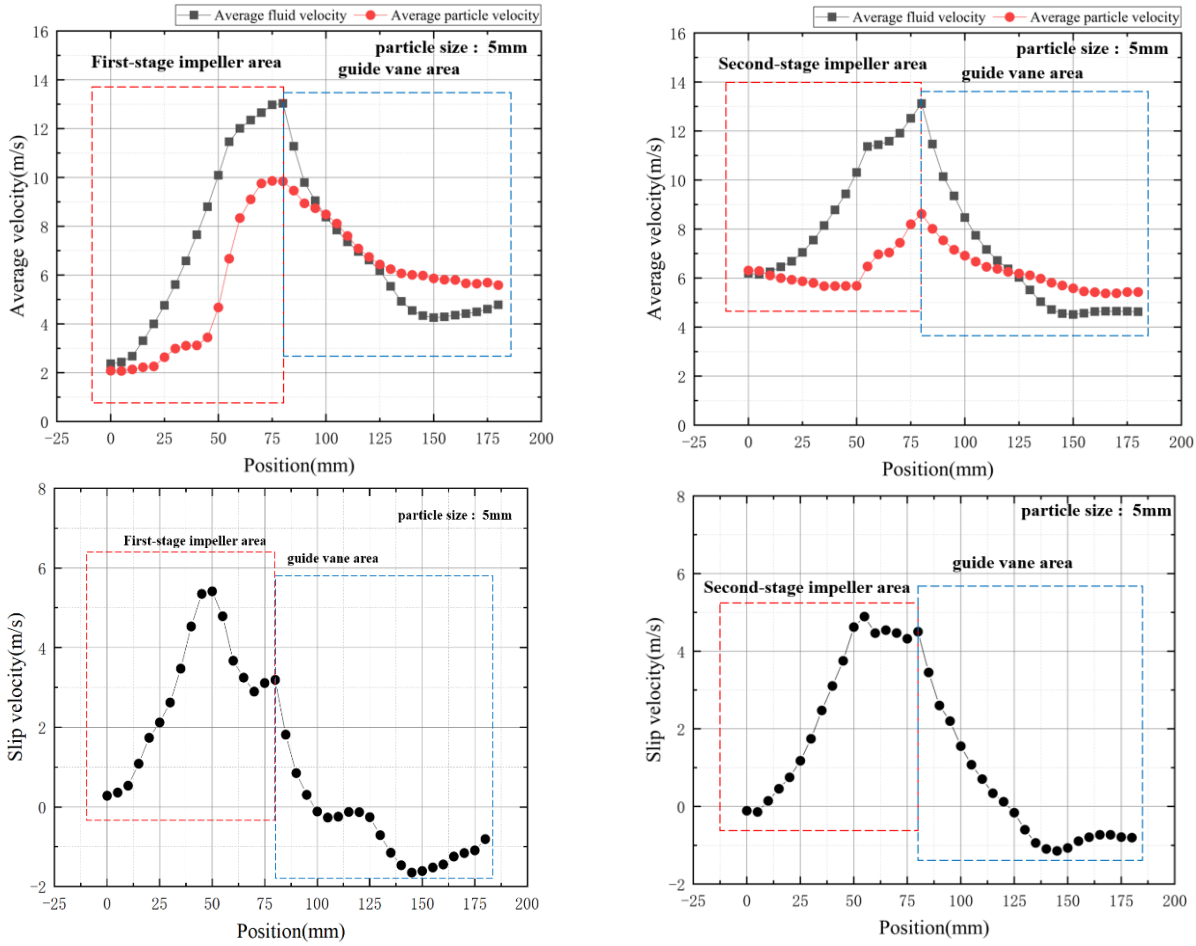

(a) Average particle-fluid velocity and velocity slip in the first stage.

(b) Average particle-fluid velocity and velocity slip in the second stage.

Fig. 12 Average particle (5mm)-fluid velocity and velocity slip.

5 mm particles is reduced, and the particles enter the guide vane at a higher velocity, resulting in an earlier zero position of the velocity slip curve (Fig. 12(a)). The maximum negative value of the velocity slip is -1.64 m/s. The velocity curve of the 5 mm particles in the second-stage pump is similar to that of the 10 mm particles; hence it will not be described in detail.

As shown in Fig. 13, the limitation of the data statistics method causes strong oscillations in the particle velocity curve when the particle size increases to 15 mm, but the effect on the average fluid velocity is minimal. For the movement of particles, the collisions between large particles and collision with the wall inevitably increases. Hence, individual particle velocities reach singular values, which significantly affect the overall average value. The velocity of the particles in the guide vane hardly exceeds the velocity of the fluid, as shown in Figs. 13(a) and (b), where the velocity slip only has one negative value in the middle and rear sections of the guide vane.

To compare the performance of the three particles in the slurry transport pump, this section further analyzed the slip velocity relationship between the first and second stages and presented the results in Fig.14. The velocity-slip curves of the three particles were found to be similar in both the first and second stages. Because the two-phase flow in the second-stage impeller has a higher kinetic energy obtained from the first-stage pump, the velocity slip curves of the three particles were more distinct and showed less crossover. As the two-phase flow entered the guide vane, it could be observe a leftward shift of the zero point in the slip velocity curve, and a greater decrease in amplitude after the zero point for smaller particle sizes.

After analyzing and comparing the velocity slip with different particle sizes, several conclusions can be drawn: (1) The trends of velocity slip with different particles were similar. The slip velocity increased linearly with the acceleration of impeller rotation, and then decreased in amplitude when approaching the impeller outlet (50-80 mm). Finally, the slip velocity decreased after entering the guide vane until it was close to the outlet (145-180 mm). (2) The trends of velocity slip between the two stages were similar. However, the two-phase flow had higher kinetic energy when entering the second-stage pump, resulting in a decrease in the particle velocity gradient and a tendency for the slip velocity at the impeller outlet to be flat. (3) With an increase in particle size, the peak value of particle velocity slip decreased significantly, and the zero-position shifted to the left. The change in particle size had little effect on fluid velocity but increased the variation amplitude of particle velocity, resulting in the trend of velocity slip moving to the left.

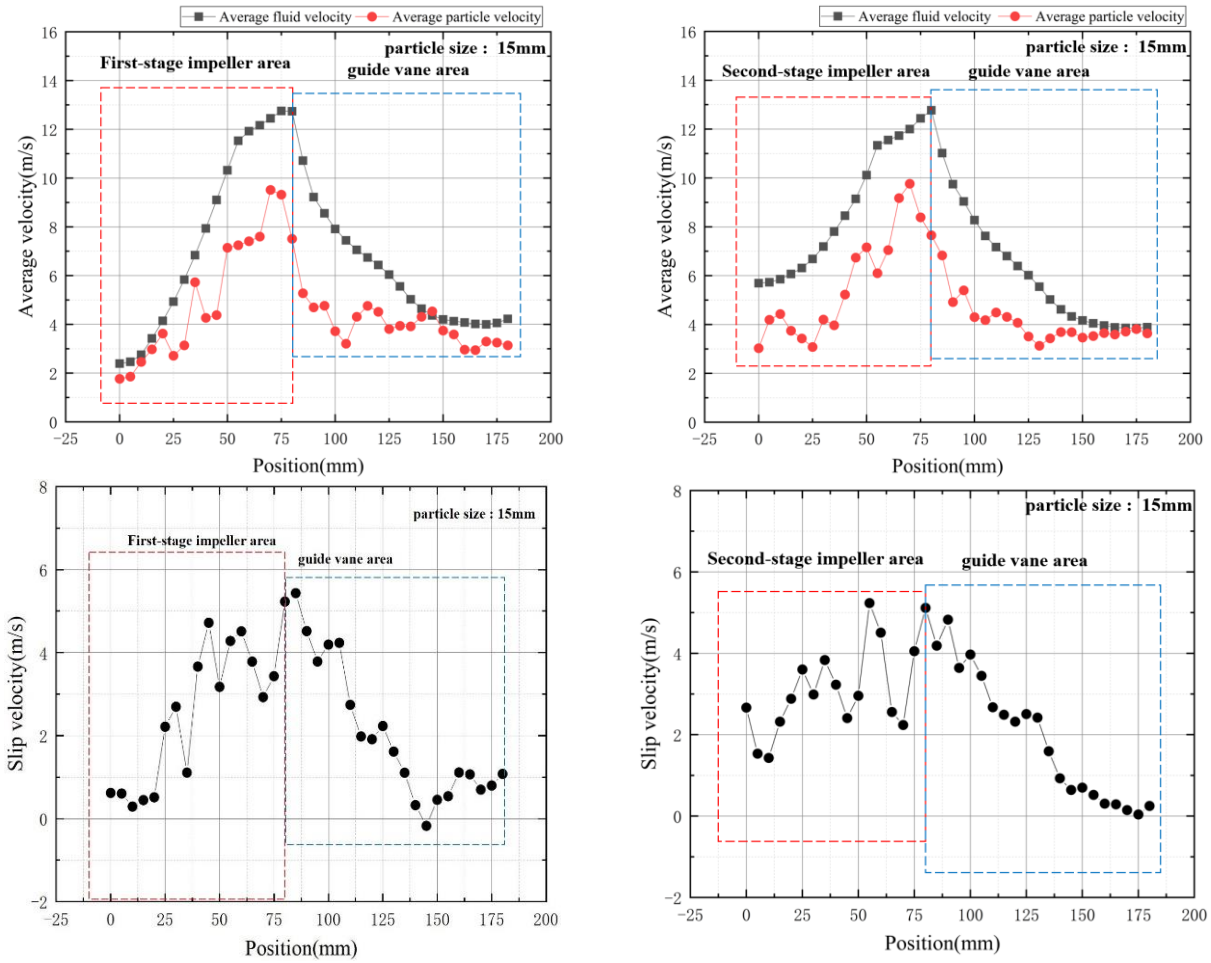

(a) Average particle-fluid velocity and velocity slip in the first stage.

(b) Average particle-fluid velocity and velocity slip in the second stage.

Fig. 13 Average particle (15 mm)-fluid velocity and velocity slip.

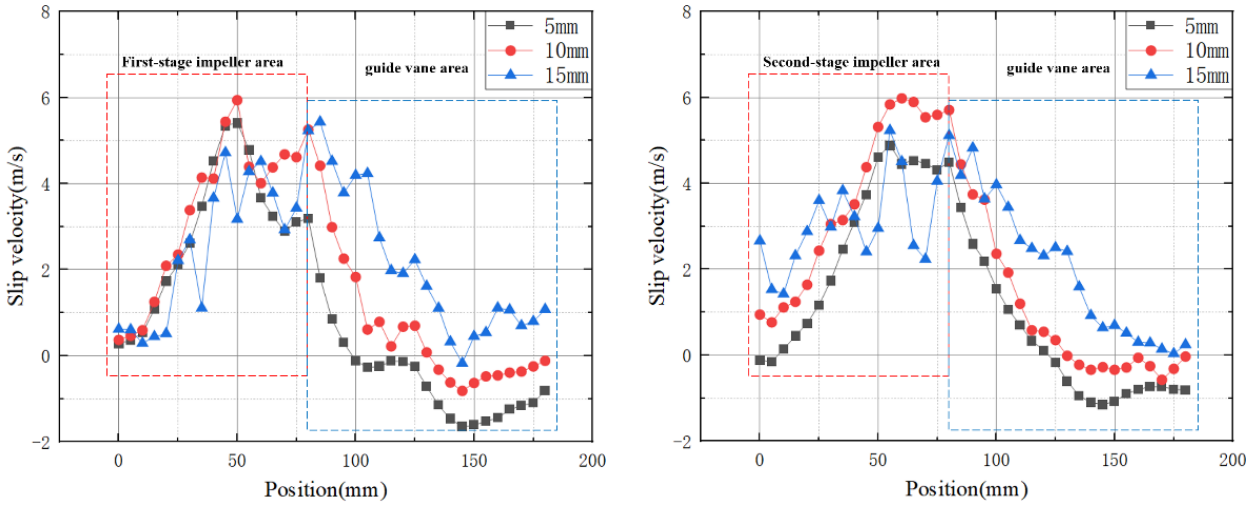

(a) Velocity slip of the three particle sizes in the first stage

(b) Velocity slip of the three particle sizes in the second stage

Fig. 14 Comparison of the velocity slips between three particle sizes.

5. CONCLUSION

In this study, the correlation between particle motion and velocity slip in a slurry pump was investigated. The main findings are summarized as follows:

(1) According to the velocity triangle of the solid and liquid phases in the impeller and Euler's equation, the theoretical pump head formula shows that a larger head is associated with a larger impeller outlet velocity slip and smaller inlet velocity slip.

(2) The particles and fluids have similar velocity curves, but the change amplitudes are quite different. With

the rotation of the impeller and diffusion of the flow channel, the velocity slip of the two-phase flow in the first-stage pump exhibits a trend of increasing and then decreasing. The velocity slip value reaches the maximum v_{max}= 6 m/s at 60 mm and decreases to zero at 130 mm, which causes particle congestion.

(3) The particle size influences the dynamic characteristics of the solid-liquid two-phase flow. The peak value of the particle velocity slip was significantly reduced, and the peak and zero-point positions shifted backward in the particle size range of 5-15 mm. Therefore, a suitable choice of the ratio of different particle sizes can improve the particle-passing ability and further improve the efficiency of the conveying system.

(4) Deep-sea particle transportation must consider the influence of particle size, concentration, and other factors on particle velocity slip. Future work requires a comprehensive and quantitative analysis of the velocity slip for better conveyance efficiency and safety.

ACKNOWLEDGEMENTS

This work was supported by Program of National Natural Science Foundation of China NO. 52071296, Joint education program of China-Middle & Eastern European countries NO. 2021129; Top-notch Talent Support Program of Zhejiang Province NO. 2019R51002 and National Key Research and Development Program NO. 2021YFC2800803, 2021YFC2801504.

CONFLICT OF INTEREST STATEMENT

All authors have no conflicts to disclose

AUTHOR CONTRIBUTIONS:

Yuwei Lv: Writing - Original Draft, Methodology, Visualization, Data Curation; Xianghui Su: Writing - Review & Editing, Supervision; Hao Yang: Formal analysis, Investigation; Jianyi Zhang: Project administration, Resources; Runkun Wang: Validation; Zuchao Zhu: Funding acquisition.

REFERENCES

Chen, B., Song, B. L., Tu, B. C., Zhang, Y. M., Li, X. J., Li, Z. G. (2021) Effect of Rotation Speed and Flow Rate on Slip Factor in a Centrifugal Pump. *Shock and Vibration*,1-4. https://doi.org/10.1155/2021/6614981

Dong, L., Cheng, T., Ding, S., & Fu, B. (2017). CFD-DEM simulation for distribution and motion feature of crystal particles in centrifugal pump. *International Journal of Fluid Machinery Systems*, 10. https://doi.org/10.5293/IJFMS.2017.10.4.378

Hong, G. J., Zhang, Q. B., & Yu, G. L. (2016). Trajectories of coarse granular sediment particles in a simplified centrifugal dredge pump model. *Advances in Mechanical Engineering*, 8(11) https://doi.org/10.1177/1687814016680143

Li, Y. L., Yuan, S. Q., Wang, X. K., Tan, S. K., & Mao. J. Y. (2016) Comparison of flow fields in a centrifugal pump among different tracer particles by particle image velocimetry. *Journal of Fluids Engineering-Transactions of the Asme*, 138. https://doi.org/10.1115/1.4032562

Li, Y. W., Liu, S. J., & Hu, X. Z. (2019). Research on rotating speed's influence on performance of Deep-Sea lifting motor pump based on DEM-CFD. *Marine Georesources & Geotechnology*, 37(8), 979-88. https://doi.org/10.1080/1064119X.2018.1514550

Liu, S. J., Li, Y. W., Hu, X. Z., & Dai, Y. (2019a, January 12-13). *Prediction of Quasi - fluid Performance in Different Volume Concentration of Deep Sea Mining*. International Conference on Intelligent Transportation, Big Data & Smart City (ICITBS), Changsha, PEOPLESR CHINA 2019.

Liu, S. J., Wen, H., Zou, W. S., Hu, X. Z., & Dong, Z., (2019b, January 12-13). *Deep-Sea Mining Pump Wear Prediction Using Numerical two-phase Flow Simulation.* International Conference on Intelligent Transportation, Big Data & Smart City (ICITBS), Changsha, PEOPLES R CHINA 2019.

Ning, C., Li, Y. L., Huang, P., Shi, H. B., Sun, H. C. (2022) Numerical analysis of single-particle motion using CFD-DEM in varying-curvature elbows. *Journal of Marine Science and Engineering*, 10. https://doi.org/10.3390/jmse10010062

Pei, Y. J., Liu, Q. Y., Wang, C., & Wang, G. R. (2021). Analytical methods and verification of impeller outlet velocity slip of solid-liquid disc pump with multi-type blades. *Arabian Journal for Science and Engineering*, 46 6835-47. https://doi.org/10.1007/s13369-020-04951-3

Peng, G. J., Chen, Q., Bai, L., Hu, Z. Q., Zhou, L., & Huang, X. (2021a) Wear mechanism investigation in a centrifugal slurry pump impeller by numerical simulation and experiments. *Engineering Failure Analysis*, 128. https://doi.org/10.1016/j.engfailanal.2021.105637

Peng, G. J., Tian, L., Chang, H., Hong, S. M., Ye, D. X., & You, B. J. (2021b) Numerical and experimental study of hydraulic performance and wear characteristics of a slurry pump. *Machines*, 9. https://doi.org/10.3390/machines9120373

Su, X., Tang, Z., Li, Y., Zhu, Z., & Balaz, P. J. E. (2020). Research of particle motion in a two-stage slurry transport pump for deep-ocean mining by the CFD-DEM method. 13(24), 6711.

https://doi.org/10.3390/en13246711

Sun, D. P., & Liu, H. X. (2022). A probability model for predicting the slip velocity of large particles in vertical pipes. *Powder Technology*, 397. https://doi.org/10.1016/j.powtec.2021.117102

Tang, C., & Kim, Y. J. (2020). CFD-DEM simulation for the distribution and motion feature of solid particles in single-channel pump. *Energies*, 13(19). https://doi.org/10.3390/en13194988

Wei, Z. B. (1997). Study on two-phase flow theory of solid-liquid pump. *Coal Mining Machinery*, (4), 3 (in China).

Wen, H., Liu, S. J., Zou, W. S., Hu, X. Z., & Dong, Z. (2019, January 12-13). *Effects of Particle Diameter on Erosion Wear Characteristic of Deep-Sea Mining Pump.* International Conference on Intelligent Transportation, Big Data & Smart City (ICITBS), Changsha, Peoples R China 2019.